City Research Online

City, University of London Institutional Repository

On the boundary-layer structure of cavity flow in a porous medium driven by differential heating

By P. G. DANIELS and M. PUNPOCHA†

Centre for Mathematical Science, City University, Northampton Square, London EC1V 0HB, UK

This paper describes the boundary-layer structure of flow through a porous medium in a two-dimensional rectangular cavity driven by differential heating of the upper surface. The lower surface and sidewalls of the cavity are thermally insulated. In the limit of large Darcy–Rayleigh number, the solution involves a horizontal boundary layer near the upper surface where the main thermal gradients occur. For a monotonic temperature distribution at the upper surface, these drive fluid to the colder end of the cavity where it descends within a narrow vertical boundary layer before returning to the horizontal layer. The horizontal and vertical layers form an interactive system which is solved by a combination of asymptotic analysis and numerical computation. A complete solution is obtained for the case of a quadratic temperature distribution at the upper surface. The solution of the interactive boundary-layer system determines the almost constant temperature in the core region below the horizontal and vertical layers, which contains relatively weak variations in both the thermal and velocity fields.

1. Introduction

Porous media play an important role in many areas of current application, including geothermal energy systems, oil and gas recovery, and the spread of pollutants in groundwater. In many cases of practical interest, the Darcy–Rayleigh number R, which characterizes the importance of buoyancy forces relative to frictional forces, is large. In a previous paper (Daniels & Punpocha 2004), steady-state solutions have been found for the motion generated within a two-dimensional rectangular cavity of aspect ratio L (width/height) by differential heating of the upper surface. If the heating is monotonic and the other three walls of the cavity are thermally insulated, a single-cell circulation is generated, the centre of which moves towards the upper cold corner of the cavity as the Darcy–Rayleigh number increases. The aim of the present work is to obtain an asymptotic description of the boundary-layer structure that emerges in the limit as $R \to \infty$. The main ingredients of this structure are a horizontal boundary layer at the upper surface where the main thermal variations occur and a vertical boundary layer at the top of the sidewall adjoining the colder end of the upper surface. Fluid driven along the upper surface within the horizontal layer enters the vertical layer where it descends and then returns to the horizontal layer. Exactly how this is accomplished is an important feature of the structure to be identified here.

There have been various previous studies of boundary-layer flows in porous media. Similarity solutions of the boundary-layer equations on a heated horizontal wall

† Present address: Department of Mathematics, King Mongkut's Institute of Technology, Bangkok 10800, Thailand.

have been discussed by Cheng & Chang (1976) and Chang & Cheng (1983), whilst boundary-layer flows on a heated vertical wall have been studied by Cheng & Minkowycz (1977), Merkin (1980), Ingham, Merkin & Pop (1982), Joshi & Gebhart (1984) and Ingham & Brown (1986). For confined flows, most previous work relates to the situation where motion is driven by maintaining the sidewalls of a rectangular cavity at different constant temperatures. Weber (1975) and Walker & Homsy (1978) considered the large Darcy–Rayleigh number structure ($R \rightarrow \infty$ at fixed L) for the side-heated cavity with insulated upper and lower surfaces, where vertical boundary layers of thickness $O(R^{-1/2})$ control a horizontal stratified flow across the main core region. Blythe, Daniels & Simpkins (1982) analysed the structure of the vertical boundary layers near the corners, leading to the identification of a double structure along the horizontal surfaces consisting of layers of thickness $O(R^{-1/4})$ and $O(R^{-5/16})$ (Daniels, Blythe & Simpkins 1982) and enabling the asymptotic solution to be completed to leading order as $R \rightarrow \infty$ throughout the cavity. A numerical solution of the vertical boundary-layer problem was obtained by Daniels (1983). Further asymptotic structures for shallow cavities ($L = O(R)$ and $L = O(R^{1/2})$ as $R \rightarrow \infty$) have been discussed by Daniels, Blythe & Simpkins (1986, 1989) and for tall cavities ($L = O(R^{-1})$ and $L = O(R^{-1/2})$ as $R \rightarrow \infty$) by Ansari & Daniels (1993, 1994).

Although the present investigation is motivated partly by applications to differential heating in groundwater flows and geothermal energy systems, it is also designed to provide fundamental insight into general flow structures in cavities where the horizontal surfaces are thermally conducting. Structures of the kind identified in the insulating case by Daniels *et al.* (1982) are then no longer relevant. The simplest situation to consider initially is where only the upper surface is thermally conducting, with the other three acting passively as thermal insulators. The problem is formulated in §2 and numerical results for large values of R are briefly discussed. In §3, the main features of the proposed asymptotic structure of the solution as $R \rightarrow \infty$ are set out. This is based on an interaction between a horizontal boundary layer and a vertical boundary layer over a depth of order $R^{-1/3}$ near the upper surface of the cavity. For a monotonic temperature distribution along the upper surface, the vertical layer, of width order $R^{-2/3}$, occurs only at the colder end of the cavity. Similar structures have been described by Phillips (1991) in the context of geothermal energy reservoirs, where the flow is driven from below by a buoyancy source. Section 4 is concerned with the solution of the combined horizontal/vertical-layer system for depths small compared with $R^{-1/3}$, whilst §5 considers depths much greater than $R^{-1/3}$. The latter analysis reveals that virtually all of the fluid entrained into the vertical layer from the horizontal layer is returned to the horizontal layer, so that the entire leading-order circulation occurs within the two boundary layers near the upper surface. One implication of this is that the horizontal boundary-layer system is not parabolic (or near-parabolic) in one direction, a fact which must be taken into account in a full numerical solution of the combined horizontal/vertical-layer system described in §§6 and 7. The vertical layer also presents an interesting challenge numerically, because for certain external conditions the streamwise velocity field decays in an oscillatory fashion, generating reverse flow within the layer. The results are discussed in §8.

2. Formulation

A rectangular two-dimensional cavity $0 \leqslant x^* \leqslant d, 0 \leqslant z^* \leqslant h$ is filled with a fluid-saturated porous medium. The upper boundary $z^* = h$ is held at temperature

$$T^* = T_0^* + \Delta T \, S(x^*/d), \tag{2.1}$$

where the function $S(x^*/d)$ varies monotonically from zero at $x^* = 0$ to 1 at $x^* = d$. The vertical walls $x^* = 0$ and $x^* = d$ and the bottom wall $z^* = 0$ are thermally insulated. Subject to Darcy's law and the Oberbeck–Boussinesq approximation, steady two-dimensional motion is governed by the non-dimensional equations

$$\nabla^2 \psi = -R \frac{\partial T}{\partial x}, \tag{2.2}$$

$$\nabla^2 T = \frac{\partial(T, \psi)}{\partial(x, z)}, \tag{2.3}$$

where $\psi(x, z)$ is the streamfunction non-dimensionalized by the thermal diffusivity κ, $T(x, z)$ is the temperature measured relative to T_0^* and non-dimensionalized by ΔT, (x, z) are Cartesian coordinates non-dimensionalized by h and R is the Darcy–Rayleigh number defined by

$$R = K g \bar{\beta} \Delta T h / \kappa \nu, \tag{2.4}$$

where K is the permeability, $\bar{\beta}$ is the coefficient of thermal expansion, ν is the kinematic viscosity and g is the acceleration due to gravity. The non-dimensional velocity components in the x, z directions are given by

$$u = \frac{\partial \psi}{\partial z}, \quad w = -\frac{\partial \psi}{\partial x}, \tag{2.5}$$

respectively.

The cavity walls are assumed to be impermeable, so that the boundary conditions are

$$\psi = \frac{\partial T}{\partial x} = 0 \quad \text{on} \quad x = 0, L, \tag{2.6}$$

$$\psi = \frac{\partial T}{\partial z} = 0 \quad \text{on} \quad z = 0 \tag{2.7}$$

and

$$\psi = 0, \quad T = S(x/L) \quad \text{on} \quad z = 1. \tag{2.8}$$

Solutions of the problem defined by (2.2), (2.3) and (2.6)–(2.8) depend on the Darcy–Rayleigh number R and the aspect ratio $L = d/h$, and also on the specific form of the temperature profile $S(x/L)$, which is taken to be regular at $x = 0$. Note that because the bottom wall and sidewalls of the cavity are thermally insulated, the total heat flux through the upper surface is zero:

$$\int_0^L \frac{\partial T}{\partial z}(x, 1) \, dx = 0. \tag{2.9}$$

Numerical solutions of the above problem have been reported by Daniels & Punpocha (2004) for a wide range of Darcy–Rayleigh numbers and aspect ratios, and for both quadratic and cosine temperature distributions at the upper surface. These show that as the Darcy–Rayleigh number increases, a boundary-layer structure emerges, with the main variation in temperature occurring near the upper surface and driving a single-cell circulation about a point near the upper cold corner. The results are qualitatively similar for different forms of S. Figure 1 shows results obtained for the quadratic profile

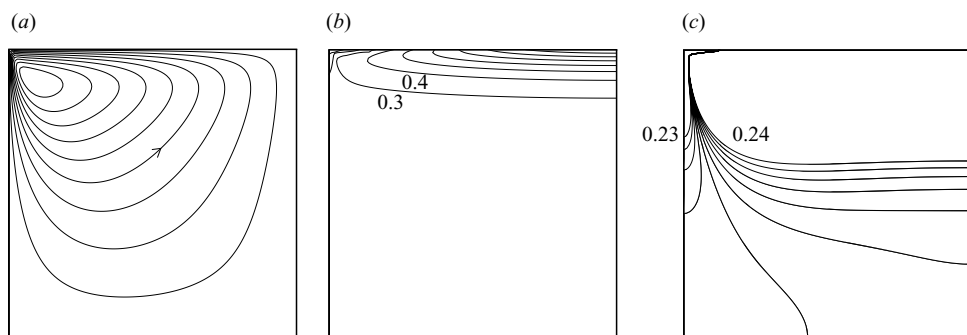$$S(x/L) = 1 - \left(1 - \frac{x}{L}\right)^2, \tag{2.10}$$

FIGURE 1. Numerical solutions showing the isotherms and streamlines in a square cavity ($L=1$) at $R=5000$. (*b*) and (*c*) show the isotherms at intervals of 0.1 and 0.01, respectively, the latter in the range 0.23 to 0.24 only.
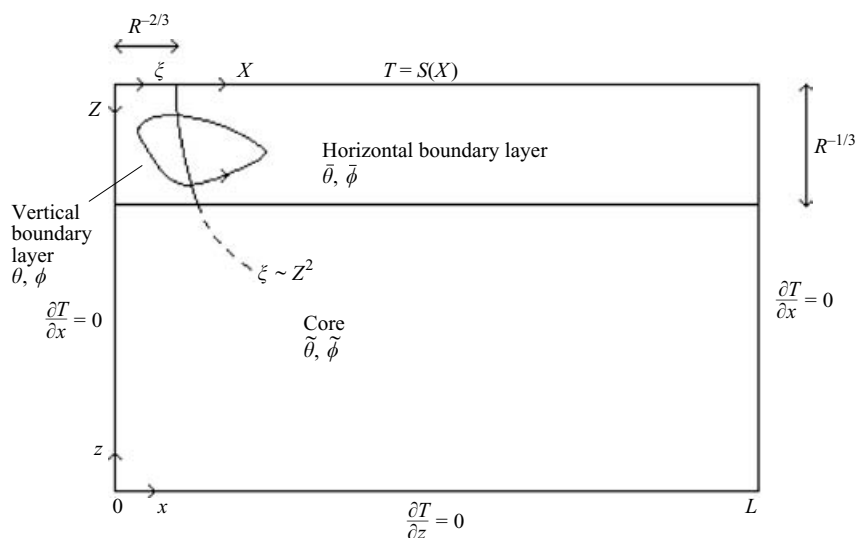

FIGURE 2. Schematic diagram showing the main features of the solution structure in the limit $R \rightarrow \infty$ and the leading-order scaled variables in each region.

with $R=5000$ and $L=1$. These indicate that most of the core region below the upper thermal layer is at a near-constant temperature of about 0.23 to 0.24.

The aim of the present work is to find an asymptotic solution of the problem in the limit as $R \rightarrow \infty$.

3. Boundary-layer structure

The main features of the asymptotic structure as $R \rightarrow \infty$ are horizontal and vertical layers of thickness $R^{-1/3}$ and $R^{-2/3}$, respectively, as in the discussion by Phillips (1991, p. 263) of plume flows in porous media driven by a distributed buoyancy source. Figure 2 shows a schematic diagram of the flow domain. Near the upper surface there is a horizontal boundary layer in which

$$T(x, z) = \bar{\theta}(X, Z) + \cdots, \quad \psi(x, z) = R^{1/3} L^{1/3} \bar{\phi}(X, Z) + \cdots, \quad (3.1)$$

where

$$x = LX, \quad 1 - z = R^{-1/3}L^{2/3}Z \tag{3.2}$$

and $\bar{\theta}$ and $\bar{\phi}$ satisfy the equations

$$\frac{\partial^2 \bar{\phi}}{\partial Z^2} = -\frac{\partial \bar{\theta}}{\partial X}, \tag{3.3}$$

$$\frac{\partial^2 \bar{\theta}}{\partial Z^2} = \frac{\partial \bar{\phi}}{\partial X}\frac{\partial \bar{\theta}}{\partial Z} - \frac{\partial \bar{\phi}}{\partial Z}\frac{\partial \bar{\theta}}{\partial X}, \tag{3.4}$$

with boundary conditions

$$\bar{\phi} = 0, \quad \bar{\theta} = S(X) \quad \text{on} \quad Z = 0, \tag{3.5}$$

$$\bar{\phi} = \frac{\partial \bar{\theta}}{\partial X} = 0 \quad \text{on} \quad X = 1, \tag{3.6}$$

$$\frac{\partial \bar{\phi}}{\partial Z} \to 0, \quad \frac{\partial \bar{\theta}}{\partial Z} \to 0 \quad \text{as} \quad Z \to \infty. \tag{3.7}$$

Here, (3.5) are the conditions at the upper surface whilst (3.6) assumes that the boundary conditions at the hotter sidewall apply directly to the horizontal boundary-layer solution. This is partly because satisfaction of $\bar{\phi}=0$ at $X=1$ also implies satisfaction of $\partial\bar{\theta}/\partial X=0$ at $X=1$, from (3.3). The conditions (3.7) at the bottom edge of the layer assume that the horizontal flow tends to zero and that the temperature approaches a constant value to be determined. A further discussion of (3.7) is given at the end of this section. Note that the scalings used in (3.1) and (3.2) allow the parameter L to be removed from the system (3.3)–(3.7).

At the colder sidewall there is a vertical boundary layer which entrains fluid from the horizontal layer. Here

$$T(x, z) = \theta(\xi, Z) + \cdots, \quad \psi(x, z) = R^{1/3}L^{1/3}\phi(\xi, Z) + \cdots, \tag{3.8}$$

where

$$x = R^{-2/3}L^{1/3}\xi \tag{3.9}$$

and θ and ϕ satisfy the equations

$$\frac{\partial^2 \phi}{\partial \xi^2} = -\frac{\partial \theta}{\partial \xi}, \quad \frac{\partial^2 \theta}{\partial \xi^2} = \frac{\partial \phi}{\partial \xi}\frac{\partial \theta}{\partial Z} - \frac{\partial \phi}{\partial Z}\frac{\partial \theta}{\partial \xi} \tag{3.10}$$

and boundary conditions

$$\phi = \theta = 0 \quad \text{on} \quad Z = 0, \tag{3.11}$$

$$\phi = \frac{\partial \theta}{\partial \xi} = 0 \quad \text{on} \quad \xi = 0, \tag{3.12}$$

$$\phi \to \phi_\infty(Z), \quad \theta \to \theta_\infty(Z) \quad \text{as} \quad \xi \to \infty. \tag{3.13}$$

Here, the condition (3.11) on θ at the upper surface follows because the function $S(x/L)$ is of order $R^{-2/3}$ on the small lateral scale of the vertical boundary layer, whilst (3.12) is the boundary condition on the sidewall. The profiles ϕ_∞ and θ_∞ at the edge of the vertical layer are to be determined as part of the solution and must match with the solution in the horizontal layer, requiring that

$$\phi_\infty(Z) = \bar{\phi}(0, Z), \quad \theta_\infty(Z) = \bar{\theta}(0, Z). \tag{3.14}$$

Note also that inclusion of the factor $L^{1/3}$ in (3.9) ensures that the parameter L does not appear in (3.10)–(3.14), so that the entire system comprising (3.3)–(3.7) and (3.10)–(3.14) is independent of L.

The horizontal and vertical boundary-layer systems interact through the matching conditions (3.14) and cannot be solved independently. In §§4 and 5, solutions of the combined system are sought for small Z and large Z, respectively, and then in §§6 and 7, a full numerical solution is described.

In order to assist in the numerical computations and to justify use of the boundary conditions (3.7), it is helpful to consider some general properties of the horizontal and vertical boundary-layer systems. A key consideration is the form of the external profiles ϕ_∞ and θ_∞. The numerical computations of figure 1 suggest that both ϕ_∞ and θ_∞ may attain local maxima at finite values of Z, with the position of the maximum of ϕ_∞ (equivalent to the centre of the eddy) below that of θ_∞. Clearly a local maximum of ϕ_∞ is inevitable if, as will be shown below, $\phi_\infty \to 0$ at the lower edge of the horizontal boundary layer. The occurrence of a maximum of θ_∞ is also supported by an exact solution of the horizontal boundary-layer system (3.3)–(3.7), in the case where S is given by (2.10), reported by Daniels & Punpocha (2004):

$$\bar{\phi} = (1 - X)\phi_0(Z), \quad \bar{\theta} = \theta_1(Z) - (1 - X)^2\theta_0(Z). \tag{3.15}$$

This represents a flow in the negative x-direction in which fluid is entrained by the horizontal boundary layer at $Z = \infty$ and transported to the vertical boundary layer. The function ϕ_0 satisfies

$$\phi_0''' + \phi_0\phi_0'' - \tfrac{3}{2}\phi_0'^2 = 0, \quad \phi_0(0) = 0, \quad \phi_0''(0) = -2 \tag{3.16}$$

and, provided $\phi_0'(0) = 1.447$, approaches a finite limiting value $\phi_0(\infty) = 1.141$ as $Z \to \infty$ with exponential decay. For other positive values of $\phi_0'(0)$, solutions of (3.16) terminate with an inverse square singularity at a finite value of Z (rather than approaching either a constant value or the alternative limiting form $\phi_0 \sim 12Z^{-1}$ as $Z \to \infty$) and are therefore discarded. The function θ_0 is given by $\theta_0 = -\phi_0''/2$ and θ_1 is the solution of $\theta_1'' + \phi_0\theta_1' = 0$ rendered unique by requiring that the total heat flux into the horizontal boundary layer at the upper surface be zero,

$$\int_0^1 \frac{\partial \bar{\theta}}{\partial Z}(X, 0)\, dX = 0, \tag{3.17}$$

a consequence of (2.9). As $Z \to \infty$, θ_1 approaches the constant value 0.229 with exponential decay.

The profiles $\phi_0(Z)$ and $\theta_1(Z) - \theta_0(Z)$ at $X = 0$ are shown in figure 3. It can be confirmed that these do not lead to a consistent solution in the vertical boundary layer, as follows. In general, the vertical boundary-layer equations, (3.10), possess solutions with exponential decay of the form

$$\theta \sim \theta_\infty + \mathrm{Re}\sum_\lambda A\, e^{-\lambda(Z)\xi}, \quad \phi \sim \phi_\infty + \mathrm{Re}\sum_\lambda B\, e^{-\lambda(Z)\xi} \quad \text{as} \quad \xi \to \infty, \tag{3.18}$$

where $A = \lambda B$ and λ is a root of the quadratic equation

$$\lambda^2 - \lambda\phi_\infty' + \theta_\infty' = 0 \tag{3.19}$$

with positive real part. Solutions of this kind were discussed by Gill (1966) in relation to the boundary-layer flow in a cavity heated from the side. In the present problem
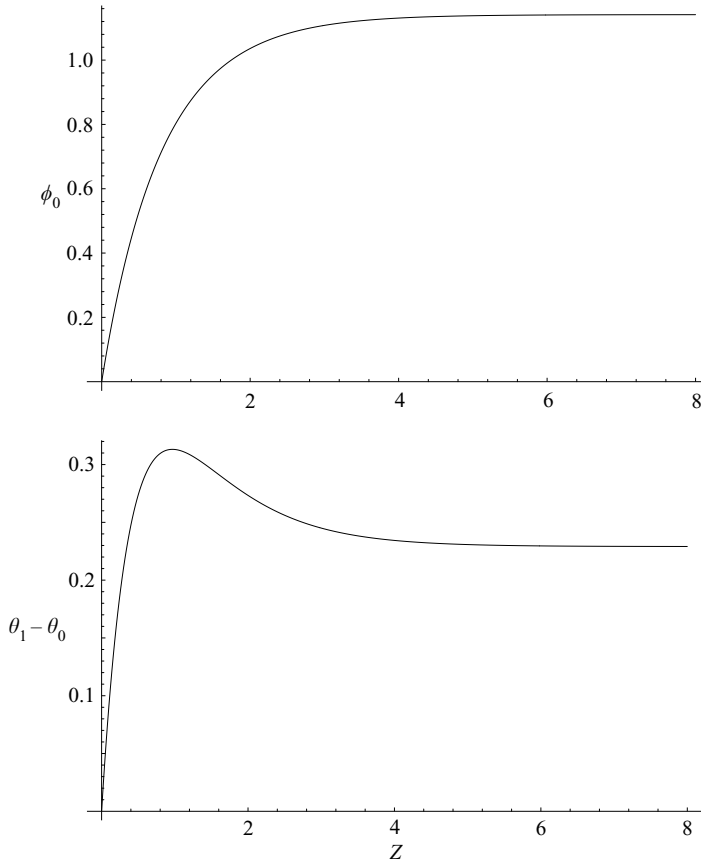
FIGURE 3. The functions ϕ_0 and $\theta_1 - \theta_0$.

the roots for λ are given by

$$\lambda = \lambda_\pm = \tfrac{1}{2}\left(\phi'_\infty \pm \left(\phi'^2_\infty - 4\theta'_\infty\right)^{1/2}\right). \tag{3.20}$$

Thus, if $\phi'_\infty > 0$ and $\theta'_\infty > 0$, both roots have positive real part, and it is possible that both ϕ_∞ and θ_∞ can be specified in the vertical boundary-layer solution as $\xi \to \infty$ (since the two wall conditions $\phi = \partial\theta/\partial\xi = 0$ at $\xi = 0$ may be satisfied by appropriate choice of $A_+ = \lambda_+ B_+$ and $A_- = \lambda_- B_-$). However, if $\theta'_\infty < 0$ (as in the region $Z > 0.96$ of figure 3), λ_+ is positive and λ_- is negative, and then at most one of the external profiles θ_∞ and ϕ_∞ can be specified when solving the vertical boundary-layer equations.

Thus, the solution (3.15) is only expected to provide a reasonable approximation in the upper part of the horizontal boundary layer and although it predicts a core temperature $\bar{\theta} \sim 0.229$ as $Z \to \infty$ in good agreement with the numerical computation of figure 1, in other respects its behaviour at large Z is not a reliable indication of the actual behaviour. In order to determine the correct asymptotic structure of the solution as $Z \to \infty$ in §5, it is necessary to investigate the relationship between the external profiles θ_∞ (with $\theta'_\infty < 0$) and ϕ_∞ generated within the vertical boundary layer. Analytical insight can be gained by considering asymptotic solutions for which

$$\phi_\infty \to a, \quad \theta_\infty \sim b + cZ^{-1} \quad \text{as} \quad Z \to \infty, \tag{3.21}$$

so that the leading terms are consistent with (3.15) (where $a = \phi_0(\infty) = 1.141$ and $b = \theta_1(\infty) = 0.229$). The algebraic correction to θ_∞ involving $c \geqslant 0$ is chosen to ensure a full balance of terms in the vertical boundary-layer equations; for (3.15) there would be an exponentially small correction as $Z \to \infty$, which can be considered as the limiting case $c \to 0$. The relevant solution of the vertical boundary-layer equations is

$$\phi \sim \tilde{F}(\tilde{\eta}), \quad \theta \sim b + Z^{-1}\tilde{G}(\tilde{\eta}), \quad Z \to \infty, \qquad (3.22)$$

where the balance of terms in (3.10) requires that $\tilde{\eta} = \xi/Z = O(1)$. Substitution into (3.10) gives

$$\tilde{G}'' + \tilde{F}'\tilde{G} = 0, \quad \tilde{F}'' = -\tilde{G}' \qquad (3.23)$$

and the requirements that $\tilde{G}(\infty) = c$ and $\tilde{F}'(\infty) = 0$ give $\tilde{F}' = c - \tilde{G}$ and thence

$$\tilde{G}'' + \tilde{G}(c - \tilde{G}) = 0, \qquad (3.24)$$

to be solved subject to

$$\tilde{G}' = 0 \quad \text{on} \quad \tilde{\eta} = 0, \quad \tilde{G} \to c \quad \text{as} \quad \tilde{\eta} \to \infty. \qquad (3.25)$$

One integration of (3.24) and use of (3.25) gives

$$\tilde{G}'^2 = \tfrac{1}{3}(\tilde{G} - c)^2(2\tilde{G} + c). \qquad (3.26)$$

Inspection of the phase plane then shows that a solution for $\tilde{G}$ consistent with (3.25) is possible with $\tilde{G}$ varying from $-c/2$ at $\tilde{\eta} = 0$ to c at $\tilde{\eta} = \infty$. This solution can be found by one further integration of (3.26) to give

$$\tilde{G} = \tfrac{1}{2}c\big(3 \tanh^2\big(c^{1/2}\tilde{\eta}/2\big) - 1\big) \qquad (3.27)$$

and the corresponding solution for $\tilde{F}'$ is

$$\tilde{F}' = \tfrac{3}{2}c \operatorname{sech}^2\big(c^{1/2}\tilde{\eta}/2\big), \qquad (3.28)$$

which indicates a downward vertical velocity ($\tilde{F}' > 0$) reaching a maximum value ($\tilde{F}' = 3c/2$) at the sidewall $\tilde{\eta} = 0$. The solution for $\tilde{F}$ is

$$\tilde{F} = 3c^{1/2} \tanh\big(c^{1/2}\tilde{\eta}/2\big) \qquad (3.29)$$

and the value of c is finally fixed by requiring that $\tilde{F}(\infty) = a$ in which case

$$a = 3c^{1/2}. \qquad (3.30)$$

This confirms that for a specified external form ϕ_∞, the corresponding variation of θ_∞ can be calculated from the vertical boundary layer (or vice versa) consistent with the fact that for $\theta'_\infty < 0$ only λ_+ is available in (3.20). More specifically, it indicates that ϕ and $\{(\theta - b)Z\}^{1/2}$ adopt the same orders of magnitude as $Z \to \infty$, equivalent to the fact that a full balance of terms is maintained in the vertical boundary-layer equations as $Z \to \infty$. This still allows for a whole family of possible solutions for orders of magnitude of ϕ and $\theta - b$ different from those assumed in (3.22) and the correct orders of magnitude must be determined by matching with a consistent structure in the horizontal boundary layer. It will be shown in §5 that this leads, essentially, to the requirement that as $Z \to \infty$ both c and a are small in the above analysis (with $a \sim c^{1/2}$) and the vertical-layer width $\tilde{\eta}(\sim c^{-1/2})$ is large. Since a is asymptotically small, this implies that all of the fluid descending in the vertical boundary layer is detrained back into the horizontal boundary layer, which must therefore contain a two-way flow satisfying $\bar{\phi} \to 0$ as $Z \to \infty$.

$\hat{k}$	0.0	0.1	0.2	0.3	0.4	0.5	0.6	0.7	0.8	0.9	1.0
$\hat{a}$	0.000	0.129	0.237	0.325	0.432	0.628	0.979	1.606	2.902	6.861	∞

TABLE 1. Values of $\hat{a}$.

4. Solution for small Z

In this section, solutions of the combined system (3.3)–(3.7)and (3.10)–(3.14) are considered for small values of Z. It is expected that

$$\phi_\infty \sim a_\infty Z + \cdots, \quad \theta_\infty \sim b_\infty Z + \cdots \quad \text{as} \quad Z \to 0, \tag{4.1}$$

where the coefficients a_∞ and b_∞ are positive and are determined by the horizontal boundary-layer solution. Thus, the vertical boundary-layer solution is expected to have the form

$$\phi = Zf(\xi) + \cdots, \quad \theta = Zg(\xi) + \cdots \quad \text{as} \quad Z \to 0. \tag{4.2}$$

Substitution into (3.10) gives

$$f' = b_\infty - g, \quad g'' = f'g - fg', \tag{4.3}$$

and from (3.12) and (3.13) the boundary conditions are

$$f = g' = 0 \quad \text{on} \quad \xi = 0, \tag{4.4}$$

$$f \to a_\infty, \quad g \to b_\infty \quad \text{as} \quad \xi \to \infty. \tag{4.5}$$

This implies that f satisfies the system

$$f''' + ff'' + f'(b_\infty - f') = 0; \quad f = f'' = 0 \quad \text{on} \quad \xi = 0, \quad f \to a_\infty \quad \text{as} \quad \xi \to \infty. \tag{4.6}$$

As $\xi \to \infty$, it is expected that

$$f \sim a_\infty + \text{Re}(k_+ \, e^{-\nu_+\xi} + k_- \, e^{-\nu_-\xi}), \tag{4.7}$$

where

$$\nu_\pm = \tfrac{1}{2}\left(a_\infty \pm \left(a_\infty^2 - 4b_\infty\right)^{1/2}\right) \tag{4.8}$$

are positive if $a_\infty^2 > 4b_\infty$, and complex conjugates with positive real part if $a_\infty^2 < 4b_\infty$. This is merely the limiting form of result (3.20) as $Z \to 0$. The constants $k_\pm$ in (4.7) must be chosen to ensure $f = f'' = 0$ at $\xi = 0$.

One method of computing f is to let

$$f(\xi) = b_\infty^{1/2} \hat{f}(\hat{\xi}), \quad \xi = b_\infty^{-1/2}\hat{\xi} \tag{4.9}$$

and then solve the system

$$\hat{f}''' + \hat{f}\hat{f}'' + \hat{f}'(1 - \hat{f}') = 0; \quad \hat{f} = \hat{f}'' = 0, \quad \hat{f}' = \hat{k} \quad \text{on} \quad \hat{\xi} = 0, \tag{4.10}$$

for different values of the constant $\hat{k}$. The solution was computed outwards from the origin using a fourth-order Runge–Kutta scheme to obtain $\hat{f}(\infty) = \hat{a}(\hat{k})$. Values of $\hat{a}$ for various values of $\hat{k}$ in the range $0 < \hat{k} \leqslant 1$ are shown in table 1 and typical solutions for the function $\hat{f}$ are shown in figure 4. For $\hat{k} \geqslant 1$, $\hat{f}$ continues to increase with $\hat{\xi}$ and a constant limit is not achieved as $\hat{\xi} \to \infty$.

From (4.6), it is required that $a_\infty = b_\infty^{1/2}\hat{a}(\hat{k})$ so that for given values of a_∞ and b_∞ the relevant value of $\hat{a}$ is determined by

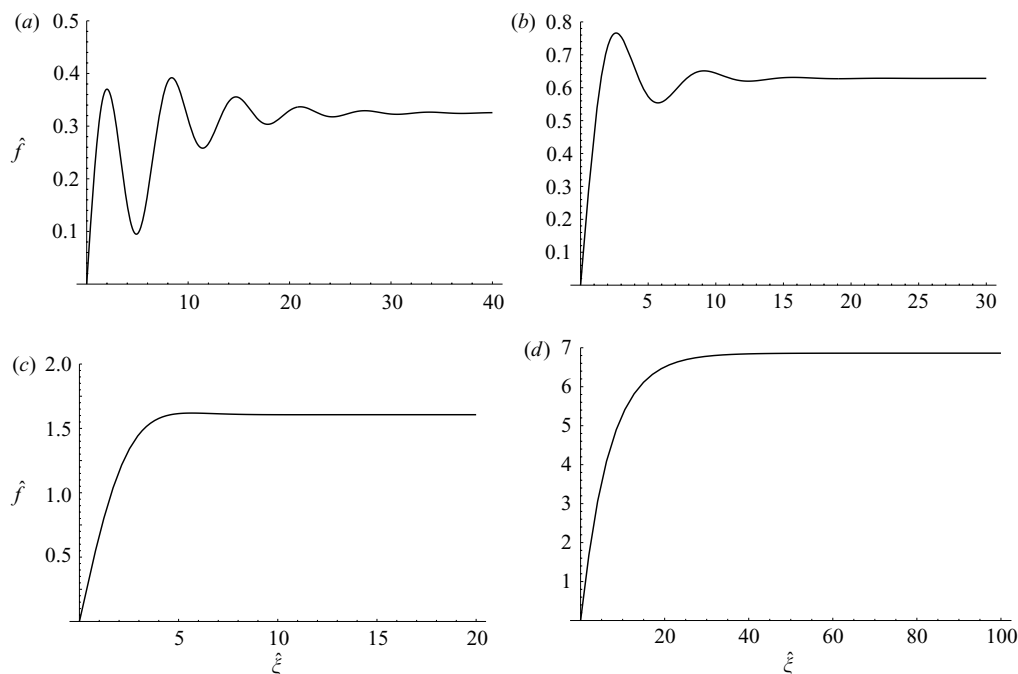$$\hat{a} = a_\infty b_\infty^{-1/2} \tag{4.11}$$

FIGURE 4. The function $\hat{f}$ for various values of $\hat{k}$. (a) $\hat{k} = 0.3$. (b) $\hat{k} = 0.5$. (c) $\hat{k} = 0.7$.
(d) $\hat{k} = 0.9$.

and (in principle) the corresponding value of $\hat{k}$ is determined from table 1. Note the oscillatory behaviour of the solution for $\hat{f}$ for $\hat{a} < 2$, consistent with the existence of complex conjugate roots of (4.8) in this case. As the entrainment velocity decreases, or the negative thermal gradient increases ($\hat{a} \to 0$) this spatial oscillation is a manifestation of the Darcy–Rayleigh instability, but for the computations reported here, the value of $\hat{a}$ is sufficiently large to avoid any significant oscillatory behaviour (see §7). Note also that as $\hat{k}$ approaches the value 1, $\hat{f}$ approaches the exact solution $\hat{f} = \hat{\xi}$ of (4.10) and in this case $\hat{a} \to \infty$.

For the horizontal boundary-layer solution (3.15), $a_\infty = \phi_0'(0) = 1.447$ and $b_\infty = (\phi_0'(0))^2/2 = 1.047$, so that this solution corresponds to the case $\hat{a} = \sqrt{2}$ where the behaviour at the edge of the vertical boundary layer is oscillatory. Note also that for the marginal case $\hat{a} = 2$, the two roots $\nu_\pm$ in (4.8) are equal and then the two exponentials in (4.7) are replaced by the form $(k_+ + k_-\xi)\,\mathrm{e}^{-\nu_+\xi}$.

The solution for small Z obtained here confirms that both of the external profiles ϕ_∞ and θ_∞ can be specified at the edge of the layer, consistent with the observations made in §3.

5. Solution for large Z

In this section, solutions of the combined system (3.3)–(3.7) and (3.10)–(3.14) are considered for large values of Z. In the vertical boundary layer, a generalization of (3.22) is assumed in which

$$\phi \sim Z^{-\alpha} F(\eta), \quad \theta \sim b + Z^{-\beta} G(\eta) \quad \text{as} \quad Z \to \infty, \tag{5.1}$$

with $\eta = \xi/Z^\gamma$ and where α, β and γ are constants to be determined. A balance of terms in both equations (3.10) requires $\alpha = \gamma - 1$ and $\gamma = \beta - \alpha$ from which it follows that

$$2\alpha = \beta - 1. \tag{5.2}$$

This is equivalent to the balance between ϕ and $\{(\theta - b)Z\}^{1/2}$ discussed at the end of §3; the solution (3.22) corresponds to the special case $\alpha = 0, \beta = 1, \gamma = 1$. Now consider the horizontal boundary layer where in order to match with (5.1) it must be assumed that

$$\bar{\phi} \sim Z^{-\alpha} p(X), \quad \bar{\theta} \sim b + Z^{-\beta} q(X) \quad \text{as} \quad Z \to \infty. \tag{5.3}$$

A balance of terms in the horizontal boundary-layer equation (3.3) requires

$$\beta = \alpha + 2. \tag{5.4}$$

From (5.2) and (5.4), it now follows that $\alpha = 1$ and $\beta = 3$, and also that $\gamma = 2$. For these values of α and β, a full balance also occurs in the horizontal boundary-layer equation (3.4), so that there is a balance between conduction and convection as $Z \to \infty$ in both the vertical and horizontal layers.

Proceeding on the assumption that

$$\phi_\infty \sim p_0 Z^{-1}, \quad \theta_\infty \sim b + q_0 Z^{-3} \quad \text{as} \quad Z \to \infty, \tag{5.5}$$

where p_0 and q_0 are constants to be determined, substitution of (5.1) into (3.10) with $\alpha = 1, \beta = 3, \gamma = 2$ shows that the vertical boundary-layer functions F and G satisfy the equations

$$F' = q_0 - G, \quad G'' = FG' - 3F'G. \tag{5.6}$$

Elimination of G then shows that F satisfies the third-order system

$$F''' - FF'' - 3F'(q_0 - F') = 0, \tag{5.7}$$

with boundary conditions

$$F = F'' = 0 \quad \text{on} \quad \eta = 0, \quad F' \to 0 \quad \text{as} \quad \eta \to \infty. \tag{5.8}$$

The constant q_0 is assumed positive and can be eliminated using the transformation

$$F(\eta) = q_0^{1/2} \hat{F}(\hat{\eta}), \quad \eta = q_0^{-1/2} \hat{\eta}, \tag{5.9}$$

to obtain

$$\hat{F}''' - \hat{F}\hat{F}'' + 3\hat{F}'(\hat{F}' - 1) = 0, \tag{5.10}$$

$$\hat{F} = \hat{F}'' = 0 \quad \text{on} \quad \hat{\eta} = 0, \quad \hat{F}' \to 0 \quad \text{as} \quad \hat{\eta} \to \infty. \tag{5.11}$$

The solution of this system is expected to yield the numerical value of $\hat{F}(\infty) = \mu$, say, in which case (5.9) and (5.5) together imply that p_0 and q_0 are related by the equation

$$p_0 = \mu q_0^{1/2}. \tag{5.12}$$

However, it is not obvious that a solution exists for which $\hat{F}$ approaches a constant value as $\hat{\eta} \to \infty$, given that $\hat{F} = \hat{\eta}$ is one solution of (5.10) which satisfies both conditions at the origin, but does not have the required behaviour at large $\hat{\eta}$. Computations using a shooting method based on a fourth-order Runge–Kutta scheme and starting from the two conditions at the origin together with $\hat{F}'(0) = \hat{k}_0$ were inconclusive and generally approach the singular form

$$\hat{F} \sim 6(\hat{\eta} - \hat{\eta}_0)^{-1} \quad \text{as} \quad \hat{\eta} \to \hat{\eta}_0-, \tag{5.13}$$
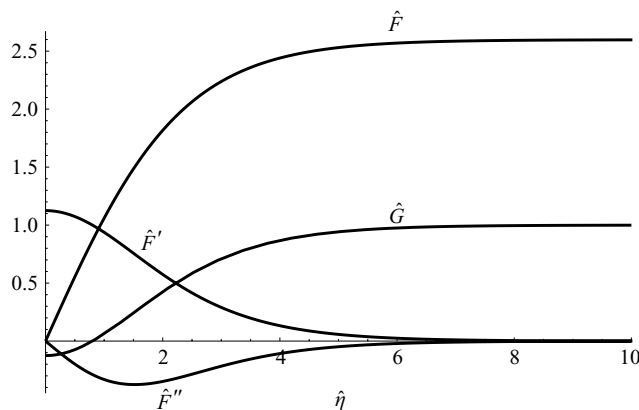
FIGURE 5. The functions $\hat{F}$, $\hat{F}'$, $\hat{F}''$ and $\hat{G}$.

with the value of $\hat{\eta}_0$ depending on $\hat{k}_0$. Nevertheless, there are solutions for which

$$\hat{F} \sim \mu + \mu_1 \, e^{-c_1\hat{\eta}} + \mu_2 \, e^{-2c_1\hat{\eta}} \quad \text{as} \quad \hat{\eta} \to \infty. \tag{5.14}$$

Substitution into (5.10) shows that if $\mu > 0$, a non-zero solution for c_1 is possible with

$$c_1 = \tfrac{1}{2}\left(-\mu + (\mu^2 + 12)^{1/2}\right) \tag{5.15}$$

and

$$\mu_2 = \mu_1^2 c_1 \left(4c_1^2 + 2\mu c_1 - 3\right)^{-1}. \tag{5.16}$$

If (5.14) were assumed to hold for all $\hat{\eta}$ and the two boundary conditions applied at $\hat{\eta} = 0$, then the arbitrary constants μ and μ_1 are determined as $\mu = 27/\sqrt{858}$ and $\mu_1 = -4\mu/3$ (with $c_1 = \sqrt{39/22}$ and $\mu_2 = \mu/3$). The actual solution was found using this as an initial guess and shooting backwards from a suitably large value $\hat{\eta}_\infty$ of $\hat{\eta}$ using a fourth-order Runge–Kutta scheme. At $\hat{\eta} = 0$, the required zeros of $\hat{F}(0)$ and $\hat{F}''(0)$ were located by Newton iteration. This gave

$$\mu = 2.598, \tag{5.17}$$

with $\hat{F}'(0) = 1.125$. The solution for $\hat{F}$ is shown in figure 5, along with $\hat{F}'$, $\hat{F}''$ and the corresponding temperature profile

$$\hat{G} = 1 - \hat{F}', \tag{5.18}$$

where $G = q_0\hat{G}(\hat{\eta})$. Note that $\hat{G}(0) = -0.125$, so that the wall temperature at $x = 0$ is an increasing function of Z, which is physically plausible. The solution for $\hat{F}$ was checked by computing outwards from $\hat{F} = \hat{F}'' = 0$, $\hat{F}' = 1.125$ at $\hat{\eta} = 0$; the effect of changing $\hat{F}'(0)$ by a small amount, either up or down, is to provoke the onset of the singularity (5.13). This is delayed to higher values of $\hat{\eta}$ by a fine adjustment of $\hat{F}'(0)$, but the solution is extremely sensitive to its value, making the backward shooting method a much better option.

Next consider the horizontal boundary layer. With $\alpha = 1$ and $\beta = 3$, substitution of (5.3) into (3.3), (3.4) shows that the functions $p(X)$ and $q(X)$ satisfy the equations

$$2p = -q', \quad 12q = pq' - 3p'q. \tag{5.19}$$

The boundary conditions (3.6) are equivalent to the requirement that

$$p = q' = 0 \quad \text{on} \quad X = 1. \tag{5.20}$$

Elimination of p in (5.19) gives a second-order equation for q which can be integrated once to give

$$q'^2 = 48q - Cq^{2/3}, \tag{5.21}$$

where C is a constant. Since $q' = -2p = -2p_0$ at $X = 0$ and $q = q_0$ at $X = 0$ it follows that

$$C = 48q_0^{1/3}\left(1 - \tfrac{1}{12}\mu^2\right), \tag{5.22}$$

where p_0 has been replaced in terms of q_0 using (5.11). Since $\mu = 2.598$, it follows that C is positive. Another integration of (5.21), making use of the fact that $q = q_0$ at $X = 0$, gives

$$\int_{q_0}^{q} \left(48q - Cq^{2/3}\right)^{-1/2} \mathrm{d}q = -X, \tag{5.23}$$

where it is assumed that $q' \leqslant 0$ so that $p > 0$ in (5.19), consistent with the fact that the streamfunction should be positive. The integral can be evaluated by the substitution

$$v = \left(\frac{q}{q_0}\right)^{1/3} - 1 + \tfrac{1}{12}\mu^2 \tag{5.24}$$

to obtain

$$3(q_0/48)^{1/2} \int_{\mu^2/12}^{v} \left(v + 1 - \tfrac{1}{12}\mu^2\right) v^{-1/2} \,\mathrm{d}v = -X. \tag{5.25}$$

From the boundary condition (5.20) at $X = 1$, together with (5.21), it follows that

$$q(1) = \left(\tfrac{1}{48}C\right)^3 = \left(1 - \tfrac{1}{12}\mu^2\right)^3 q_0, \tag{5.26}$$

so that $v = 0$ at $X = 1$. Setting $X = 1$ in (5.25) now determines the value of q_0 as

$$q_0 = 16\mu^{-2}\left(1 - \tfrac{1}{18}\mu^2\right)^{-2} = 6.068 \tag{5.27}$$

and from (5.12) the corresponding value of p_0 is

$$p_0 = \mu q_0^{1/2} = 6.400. \tag{5.28}$$

The complete solution for $q(X)$ is given implicitly from (5.25) as

$$\left(\tfrac{1}{12}q_0\right)^{1/2} v^{1/2}\left(v + 3 - \tfrac{1}{4}\mu^2\right) = 1 - X, \tag{5.29}$$

where q is related to v by (5.24), and is shown in figure 6. The corresponding solution for $p(X)$ is then given from (5.19) and (5.21) as

$$p = (12q_0)^{1/2} v^{1/2}\left(v + 1 - \tfrac{1}{12}\mu^2\right) \tag{5.30}$$

and is also shown in figure 6. It is noted from (5.26) that $q(1) = 0.508$ so that the wall temperature at $x = L$ given by (5.3) is a decreasing function of Z, consistent with the maximum value $(\bar{\theta} = 1)$ which occurs at the upper corner $x = L$, $z = 1$.

The asymptotic structure found here provides a consistent solution as $Z \to \infty$ across both the horizontal and vertical boundary-layer regions. The structure is consistent with the requirement that the net vertical heat flux (which vanishes for any horizontal section of the cavity) is zero and supports the idea that the main circulation, at the order $R^{1/3}$ level of the streamfunction, is completed within these layers. However, the slow algebraic decay of the streamfunction indicates that the depth of the layers is numerically large on the vertical scale $R^{-1/3}$, explaining why the circulation at $R = 5000$ in figure 1 still extends significantly throughout the cavity. The width of the vertical boundary layer, on the horizontal scale $R^{-2/3}$, increases as the square
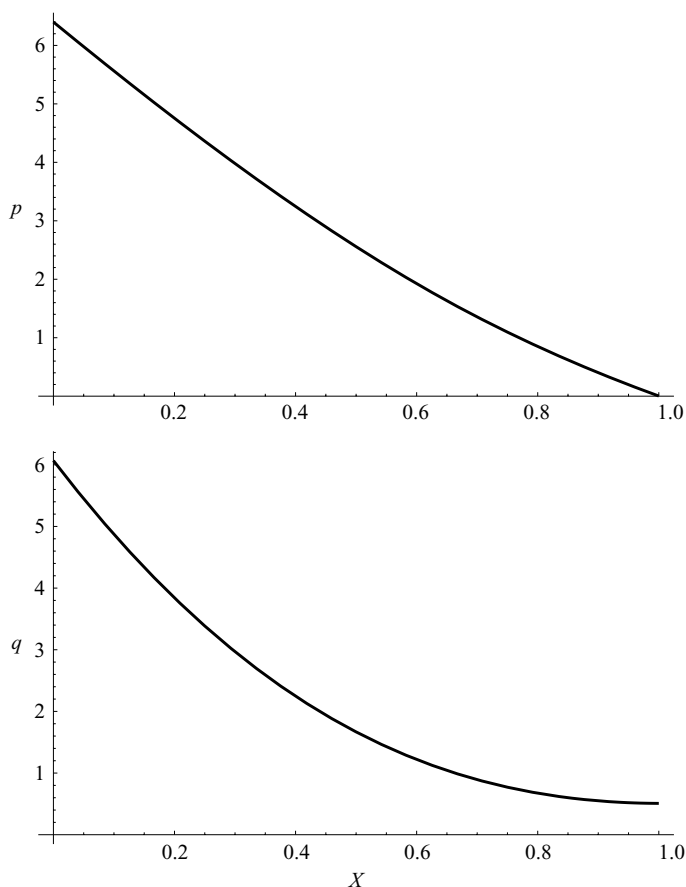
FIGURE 6. The functions p and q.

of its depth, consistent with the divergent behaviour of the streamlines near the colder sidewall in figure 1. The downward velocity in the vertical boundary layer is inversely proportional to the cube of the depth, the reduction being achieved by the detrainment of fluid back into the horizontal boundary layer. As far as the temperature is concerned, the correction to the constant value b as $Z \to \infty$ is negative near the cold sidewall and positive elsewhere, with the precise point at which $T = b$ occurring within the vertical boundary layer. Since $q(X)$ is a decreasing function of X, isotherms with $T > b$ emanating from within the vertical boundary layer turn upwards near the base of the horizontal boundary layer, consistent with the behaviour observed in figure 1.

6. Numerical scheme

A numerical scheme for solving the combined boundary-layer system (3.3)–(3.7) and (3.10)–(3.14) is now described.

In the horizontal layer, the equations (3.3), (3.4) are of parabolic type, but not in one direction. This can be understood by considering their forms near $X = 0$. If locally the functional relation between $\bar{\theta}$ and $\bar{\phi}$ is written as $\bar{\theta} = \bar{F}(\bar{\phi})$, so that $\partial\bar{\theta}/\partial X = \bar{F}'\partial\bar{\phi}/\partial X$, then for $Z < Z_0$ (where $\bar{F}' > 0$, since $\bar{\theta}$ and $\bar{\phi}$ are both increasing functions of Z)

equation (3.3) is parabolic in the negative X direction. If $Z_1(>Z_0)$ is defined as the value of Z at which ϕ_∞ reaches its maximum value, then for $Z_0 < Z < Z_1$, $\bar{F}' < 0$ (since $\bar{\theta}$ decreases as $\bar{\phi}$ increases) and so (3.3) is locally parabolic in the positive X direction; for $Z > Z_1$, $\bar{F}' > 0$ (since $\bar{\theta}$ and $\bar{\phi}$ both decrease with Z) and so (3.3) is parabolic in the negative X direction. The heat equation (3.4) is parabolic in the negative X direction for $Z < Z_1$ (since $\bar{u} = -\partial\bar{\phi}/\partial Z < 0$ there) and the positive X direction for $Z > Z_1$ (where $\bar{u} > 0$).

Thus both equations (3.3), (3.4) are parabolic in the negative X direction for $Z < Z_0$, while for $Z > Z_0$ they are parabolic in opposite directions. This corresponds precisely with the ability of the vertical boundary layer to accept specification of both ϕ_∞ and θ_∞ in $Z < Z_0$, but only one of these in $Z > Z_0$. These considerations mean that it is impractical to solve the horizontal boundary-layer equations using a parabolic marching scheme and instead the solution was allowed to evolve to a steady state by solving the artificial time-dependent system

$$\frac{\partial\bar{\phi}}{\partial t} = \frac{\partial^2\bar{\phi}}{\partial Z^2} + \frac{\partial\bar{\theta}}{\partial X}, \quad \frac{\partial\bar{\theta}}{\partial t} = \frac{\partial^2\bar{\theta}}{\partial Z^2} - \frac{\partial\bar{\phi}}{\partial X}\frac{\partial\bar{\theta}}{\partial Z} + \frac{\partial\bar{\phi}}{\partial Z}\frac{\partial\bar{\theta}}{\partial X}, \tag{6.1}$$

with $\bar{\phi}$ and $\bar{\theta}$ regarded as functions of X, Z and time t. The boundary conditions applied in the Z direction are

$$\bar{\phi} = 0, \quad \bar{\theta} = S(X) \quad \text{on} \quad Z = 0 \tag{6.2}$$

and

$$\bar{\phi} \sim (Z+D)^{-1}p(X), \quad \bar{\theta} \sim b + (Z+D)^{-3}q(X) \quad \text{as} \quad Z \to \infty, \tag{6.3}$$

where $p(X)$ and $q(X)$ are the functions determined in §5. Note that a constant D is incorporated as a possible origin shift in the Z direction – the asymptotic solution found in §5 is actually an exact solution of the equations and the origin shift represents a correction to the solution as $Z \to \infty$ which, like b, can be expected to depend on the precise form of $S(X)$. It is important to allow for this if the system is to be solved on a finite domain in the Z direction, because of the slow decay of the streamfunction. The other boundary conditions used in the solution of (6.1) are

$$\bar{\phi} = \frac{\partial\bar{\theta}}{\partial X} = 0 \quad \text{on} \quad X = 1 \tag{6.4}$$

and

$$\bar{\theta} = \theta_\infty(Z) \quad \text{on} \quad X = 0 \quad \text{for} \quad Z > Z_0. \tag{6.5}$$

The equations (6.1) were discretized on a uniform mesh in X and Z in the region $0 \leqslant X \leqslant 1, 0 \leqslant Z \leqslant Z_\infty$ where Z_∞ is a suitably large outer boundary. An explicit finite-difference scheme was used, based on central differences in X and Z and a forward difference in time. This allows new values of $\bar{\phi}$ and $\bar{\theta}$ to be determined at successive time steps at all internal grid points. New values of $\bar{\phi}$ and $\bar{\theta}$ on $Z = 0$ and $Z = Z_\infty$ are determined using (6.2) and (6.3). New values of $\bar{\phi}$ and $\bar{\theta}$ on $X = 1$ are obtained using (6.4), with a quadratic extrapolation based on two internal grid points in the case of $\bar{\theta}$. No conditions are applied on $\bar{\theta}$ and $\bar{\phi}$ for $Z \leqslant Z_0$ at $X = 0$ and new values are set there by using a quadratic extrapolation of the solution at three internal grid points. The same method is used to set the new values of $\bar{\phi}$ at $X = 0$ in $Z > Z_0$; the values of the temperature in $Z > Z_0$ are fixed by (6.5).

In order to carry out the horizontal boundary-layer calculation, values of b, D, Z_0 and the function θ_∞ for $Z > Z_0$ must be specified, together with initial forms for $\bar{\phi}$ and $\bar{\theta}$ at $t = 0$. Further details of this are given below.

The next stage of the numerical scheme is to take the new steady-state profiles ϕ_∞ and θ_∞ (the latter for $Z \leqslant Z_0$ only) and use these as boundary conditions for ϕ and θ at the edge of the vertical boundary layer. The steady-state vertical boundary-layer equations (3.10) are predominantly parabolic in the Z direction, although small upward velocities can occur near the edge of the layer if the outward exponential decay is oscillatory which, according to (3.20), is the case in $Z < Z_0$ if $\theta'_\infty > \phi'^2_\infty/4$. Apart from this difficulty, it was found that the most stable way of solving the vertical boundary-layer system was to march the solution in Z from the initial profile (3.11) at $Z = 0$. The vertical boundary layer widens considerably downstream, with $\xi \sim (Z + D)^2$ as $Z \to \infty$ according to the asymptotic structure of §5 modified to incorporate the origin shift D. For this reason, a coordinate transformation $(\xi, Z) \to (s, Z)$ where $s = \xi \delta(Z)$ was used, enabling the solution to be computed on a uniform grid in s and Z over the finite domain $0 \leqslant s \leqslant s_\infty, 0 \leqslant Z \leqslant Z_\infty$. The function $\delta(Z)$ is chosen to be unity at $Z = 0$ and to have an asymptotic behaviour proportional to Z^{-2} as $Z \to \infty$ to accommodate the spreading of the layer as Z increases. Further details are given in §7. The governing equations (3.10) become

$$\delta \frac{\partial^2 \phi}{\partial s^2} + \frac{\partial \theta}{\partial s} = 0, \quad \delta \frac{\partial^2 \theta}{\partial s^2} + \frac{\partial \phi}{\partial Z} \frac{\partial \theta}{\partial s} - \frac{\partial \phi}{\partial s} \frac{\partial \theta}{\partial Z} = 0, \tag{6.6}$$

where ϕ and θ are now regarded as functions of s and Z. These are solved subject to

$$\phi = \theta = 0 \quad \text{on} \quad Z = 0, \tag{6.7}$$

$$\phi = \frac{\partial \theta}{\partial s} = 0 \quad \text{on} \quad s = 0, \tag{6.8}$$

together with

$$\phi \to \phi_\infty, \quad \theta \to \theta_\infty \quad \text{as} \quad s \to \infty \quad \text{for} \quad Z \leqslant Z_0 \tag{6.9}$$

and

$$\phi \to \phi_\infty, \quad \frac{\partial \phi}{\partial s} \to 0 \quad \text{as} \quad s \to \infty \quad \text{for} \quad Z > Z_0. \tag{6.10}$$

The equations (6.6) were converted into first-order form by introducing additional variables $\Phi = \partial \phi / \partial s$ and $\Theta = \partial \theta / \partial s$ and then the system discretized using the Crank–Nicolson method. The edge conditions (6.9) and (6.10) are applied at $s = s_\infty$. At each downstream step, the nonlinear discretized system was solved using Newton iteration. For $Z > Z_0$, the solution yields the edge profile θ_∞ and the limiting value $b = \theta_\infty(\infty)$ to be used in the boundary conditions (6.5) and (6.3) for the next computation of the horizontal boundary layer.

The computation can lead to a change in Z_0 depending on the behaviour of $\bar{\theta}$ at $X = 0$. In practice, an adjustment to Z_0 was made before each solution of the horizontal layer to ensure that $\partial \bar{\theta}(0, Z)/\partial Z$ remained zero at $Z = Z_0 -$. Such adjustments were limited to a change of at most one step length in the Z direction at any given stage. Before each computation of the horizontal layer, an adjustment was also made to the value of D. This was done by calculating $\partial \bar{\phi}/\partial Z$ at $X = 0$ and $Z = Z_\infty$ from the previous computation of the horizontal layer. The correct asymptotic behaviour requires that

$$\frac{\partial \bar{\phi}}{\partial Z}(0, Z) \sim -(Z + D)^{-2} p_0, \tag{6.11}$$

where $p_0 = 6.400$. This was used together with a relaxation factor of $1/2$ to calculate a new estimate for D, which was then used in the outer conditions (6.3) applied at $Z = Z_\infty$. The updated value of D was used in the thermal condition one iteration of

the horizontal layer after its use in the streamfunction condition. This ensures that the thermal condition applied at $Z = Z_\infty$ is consistent with that applied in (6.5) at $X = 0$.

7. Numerical results

In this section, numerical results are described for the quadratic profile (2.10). The entire scheme was started by using

$$\bar{\phi} = (1 - X)\phi_\infty(Z), \quad \bar{\theta} = \theta_\infty(Z) + (1 - (1 - X)^2)\,e^{-Z} \tag{7.1}$$

as the initial state at $t = 0$ in the horizontal layer, with $Z_0 = 0.95$ and ϕ_∞ and θ_∞ defined by

$$\phi_\infty = 1.447Z - 0.980Z^2 + 0.338Z^3, \tag{7.2}$$

$$\theta_\infty = 1.047Z - 1.164Z^2 + 0.430Z^3, \tag{7.3}$$

for $Z \leqslant Z_0$ and by

$$\phi_\infty = 6.400(Z + D)^{-1} - 0.840\,e^{-1.083(Z - Z_0)}, \tag{7.4}$$

$$\theta_\infty = 0.215 + 6.068(Z + D)^{-3} + 0.075(Z - Z_0)\,e^{-(Z - Z_0)} \tag{7.5}$$

for $Z > Z_0$, with $D = 3$. These were chosen to be consistent with the known asymptotic forms as $Z \to \infty$, to agree with the main properties of the approximate solution (3.15) for small Z, and to produce a relatively smooth join at Z_0. It is essential to start the scheme with a reasonably good initial guess in order to ensure that the vertical boundary-layer solution can be computed all the way to $Z = Z_\infty$. The initial state (7.1) was also used for subsequent computations of the horizontal boundary layer, but with ϕ_∞ and θ_∞ replaced by their latest approximations.

Various checks were carried out to test the dependency of the numerical solution on the various step sizes involved and on the implementation of the boundary conditions and initial conditions. These indicated reasonable accuracy and consistency, with the algebraic decay in Z and a limitation on s_∞ to avoid numerical instability of the vertical boundary layer probably the main sources of error. With regard to the latter, the value of $\phi'_\infty \theta'^{-1/2}_\infty$ in the region $Z < Z_0$ ranged upwards from about 1.4 at $Z = 0$, equivalent to $\hat{a} > 1.4$ in (4.11). This in turn corresponds to $\hat{k} > 0.67$ so that, as can be seen from the solution for $\hat{k} = 0.7$ in figure 4, the impact of flow reversal at the edge of the layer is small. The most accurate computations were performed with step sizes $\Delta Z = 0.05$, $\Delta X = 0.05$ and $\Delta s = 0.1$, and with outer boundaries set at $Z_\infty = 10$ and $s_\infty = 6$. In the horizontal layer, stability limitations of the explicit scheme necessitated the use of a small time step $\Delta t = 0.001$, and 10^5 time steps were used to ensure a steady-state solution was achieved. This typically emerged, to six significant figures, at around $t = 60$. In the vertical layer, the Crank–Nicolson scheme worked efficiently and a tolerance of 10^{-7} was applied to the Newton increments at each downstream step. However, it was necessary to choose the transformation function $\delta(Z)$ carefully, both to avoid instability associated with reverse flow at the edge of the layer and to ensure a sufficiently large outer boundary at all values of Z. After some experimentation, the function

$$\delta(Z) = (1 + \delta_0 Z^2)^{-1} \tag{7.6}$$

was found to be suitable with δ_0 a parameter set to the value 1 initially; the properties $\delta(0) = 1$ and $\delta \sim \delta_0^{-1} Z^{-2}$, $Z \to \infty$ are in line with the asymptotic behaviours discussed in §§4 and 5. It was found convenient to recompute the solution in the region $Z < Z_0$ and adjust δ_0 until the value of $\Phi = \partial\phi/\partial s$ at $s = s_\infty$ was zero (to at least six decimal places) at $Z = Z_0 -$. Since $\delta\Phi = \theta_\infty - \theta$, and the left-hand side is zero at

Iteration	$\theta_{\infty max}$	$\phi_{\infty max}$	b	D
0	0.3128	1.2416	0.21462	3.000
1	0.3105	0.8267	0.21185	4.413
2	0.3060	0.9217	0.21221	3.318
3	0.3083	0.8805	0.21284	4.127
4	0.3075	0.8938	0.21312	3.460
5	0.3082	0.8861	0.21308	3.904
6	0.3078	0.8907	0.21319	3.578
7	0.3081	0.8874	0.21318	3.790
8	0.3080	0.8894	0.21320	3.642
9	0.3081	0.8881	0.21321	3.737
10	0.3080	0.8889	0.21321	3.675
11	0.3081	0.8884	0.21321	3.716
12	0.3080	0.8887	0.21321	3.690
13	0.3080	0.8885	0.21321	3.706
14	0.3080	0.8886	0.21321	3.695
15	0.3080	0.8886	0.21321	3.702
16	0.3080	0.8886	0.21321	3.698

TABLE 2. Convergence of the numerical scheme showing the main properties of the solution for each complete iteration of the horizontal/vertical-layer system.
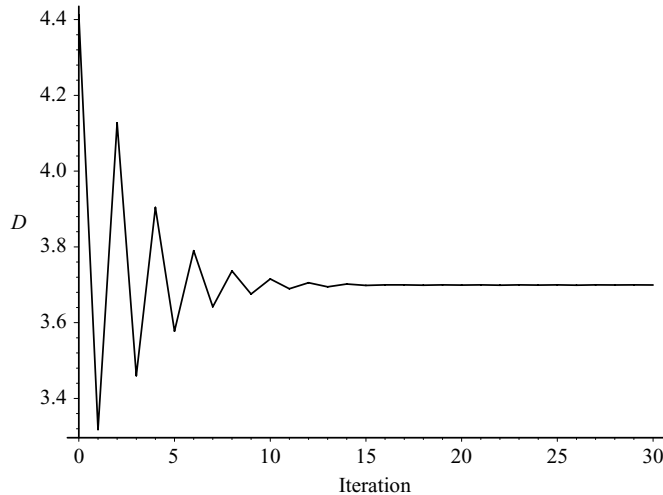

FIGURE 7. Convergence of the origin shift D with successive iterations of the horizontal/vertical-layer system.

$s = s_\infty$ for $Z > Z_0$, this ensures a smooth transition in the value of θ_∞ across $Z = Z_0$. The remainder of the vertical boundary-layer solution is then computed from $Z = Z_0$ to $Z = Z_\infty$.

Table 2 shows the behaviour of some of the main properties of the solution as a function of successive horizontal/vertical boundary-layer iterations, and serves to illustrate the rate of convergence of the scheme. Although the main features of the temperature and streamfunction fields settled down relatively quickly for moderate values of Z, the origin shift D needed 15 iterations to achieve convergence to within ± 0.01 (see also figure 7) and approached the final value
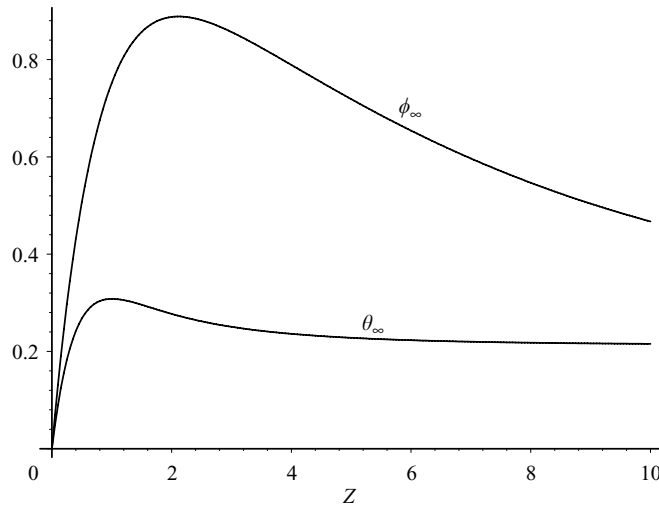
$$D = 3.700. \tag{7.7}$$

FIGURE 8. The final forms of the external profiles θ_∞ and ϕ_∞.

In the final converged state, the value of δ_0 in (7.6) was 0.894. At the edge of the vertical layer, the temperature attains a maximum value of

$$\theta_{\infty max} = 0.308 \quad \text{at} \quad Z = Z_0 = 1.00 \tag{7.8}$$

and the streamfunction attains a maximum value of

$$\phi_{\infty max} = 0.889 \quad \text{at} \quad Z = Z_1 = 2.10. \tag{7.9}$$

The predicted core temperature is

$$b = \lim_{Z \to \infty} \theta_\infty = 0.213. \tag{7.10}$$

The profiles θ_∞ and ϕ_∞ are shown in figure 8. Velocity and temperature profiles at various values of X in the horizontal boundary layer are shown in figure 9, and isotherms and streamlines in figure 10. Similar information for the vertical boundary layer is shown in figures 11 and 12.

8. Discussion

Numerical and asymptotic solutions of the combined horizontal/vertical boundary-layer system have been found, which determine the main properties of the temperature and flow fields in the cavity for general values of the aspect ratio L as $R \to \infty$. Although the numerical results of §7 are restricted to the quadratic profile, (2.10), at the upper surface, the boundary-layer solutions for other monotonic profiles $S(X)$ are expected to have the same qualitative features. In particular, the leading-order algebraic decay of the horizontal and vertical boundary-layer solutions as $Z \to \infty$, which dictates the variation of the flow and temperature fields away from the upper surface, is determined locally and is thus independent of the precise form of S. This is because the heat equation (3.4) is parabolic in the negative X direction only in the upper part of the horizontal boundary layer where $u < 0$. Had the system been parabolic in this direction throughout the layer, the decay of the solution at large Z would be expected to relate to the temperature profile $S(X)$ at $Z = 0$. However, for the problem studied here, the heat equation is parabolic in the opposite direction in the lower part
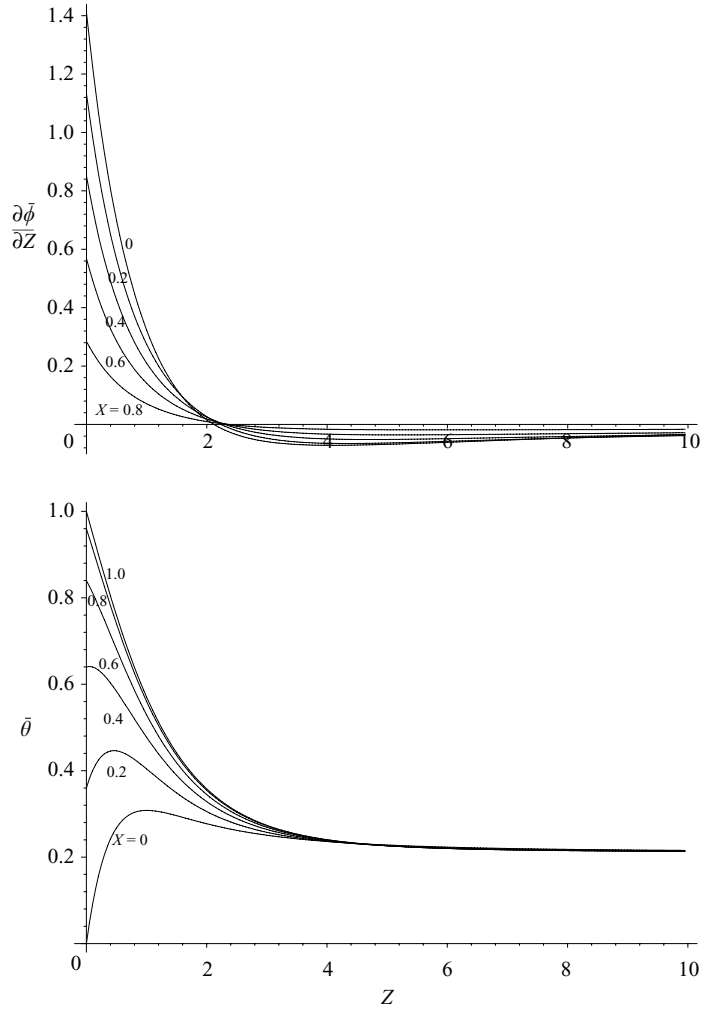
FIGURE 9. Horizontal velocity profile $\partial\bar{\phi}/\partial Z$ and temperature profile $\bar{\theta}$ at various X stations in the horizontal boundary layer.
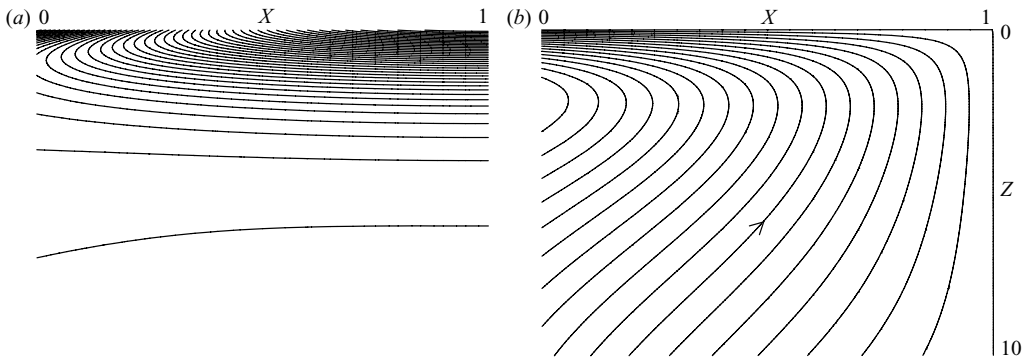
FIGURE 10. Horizontal boundary-layer solution: (*a*) isotherms, (*b*) streamlines.
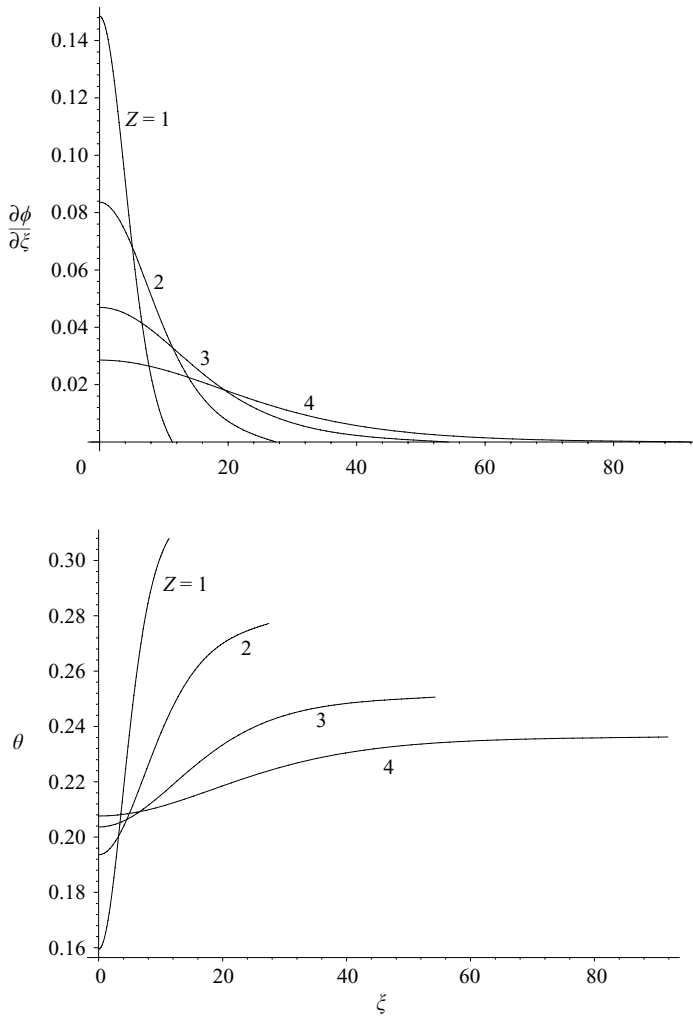
FIGURE 11. Vertical velocity profile $\partial\phi/\partial\xi$ and temperature profile θ at various Z stations in the vertical boundary layer.
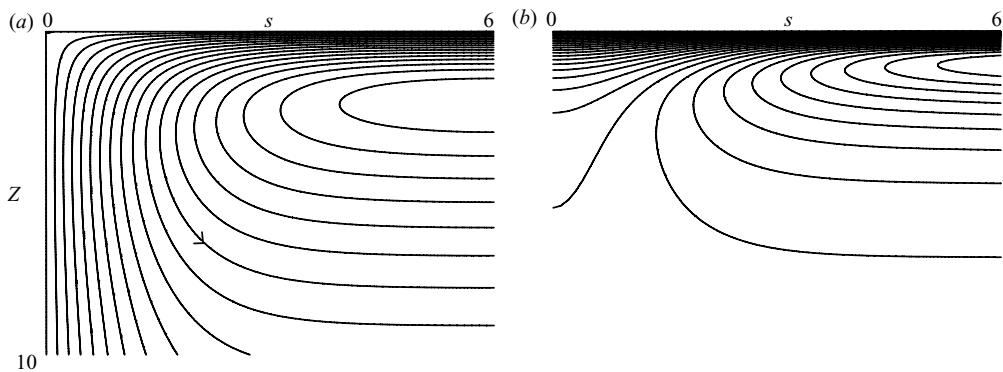

FIGURE 12. Vertical boundary-layer solution in the transformed (s, Z) plane, where the transformation function is defined by (7.6) with $\delta_0 = 0.894$: (*a*) streamlines, (*b*) isotherms.

of the layer where $u > 0$ and is more strongly influenced by information conveyed by the vertical boundary layer at $X = 0$. The precise form of S does influence the core temperature, quantitative properties of the solution within the boundary layers at finite Z and the origin shift D. According to the results of §7, for the quadratic profile (2.10), the temperature maximum at the end of the horizontal boundary layer is $T = 0.308$ and occurs at a height

$$z = 1 - R^{-1/3} L^{2/3} Z_0, \qquad (8.1)$$

where $Z_0 = 1.00$. For a square cavity ($L = 1$) and a Darcy–Rayleigh number $R = 5000$, (8.1) gives $z = 0.94$ which compares well with the numerical results of figure 1, as does the maximum value of T. According to the results of §7, the streamfunction maximum at the end of the horizontal layer occurs at

$$z = 1 - R^{-1/3} L^{2/3} Z_1, \qquad (8.2)$$

where $Z_1 = 2.10$. Again, with $L = 1$ and $R = 5000$ this gives $z = 0.88$ which compares well with the position of the centre of the eddy in figure 1 ($z = 0.90$). The value of the streamfunction at this point given by the results of §7 is

$$\psi \sim R^{1/3} L^{1/3} \phi_{\infty max}, \qquad (8.3)$$

where $\phi_{\infty max} = 0.889$. With $L = 1$ and $R = 5000$ this gives $\psi = 15.2$ compared with a value of 13.9 given by the numerical results of figure 1. Corresponding maximum values of ψ for $R = 5000$ and $L = 0.25, 0.5, 2$ and 4 computed numerically by Daniels & Punpocha (2004) are 7.7, 10.4, 18.1 and 22.7, respectively, in reasonable agreement with the values 9.6, 12.1, 19.2 and 24.1 predicted by (8.3).

Further evidence of the validity of the limiting structure proposed here is provided by the fact that the algebraic decay of the horizontal and vertical boundary-layer solutions as $Z \to \infty$ is consistent with a solution in the core region $0 \leqslant x \leqslant L, 0 \leqslant z < 1$ of the form

$$T = b + R^{-1} \tilde{\theta}(x, z) + \cdots, \quad \psi = \tilde{\phi}(x, z) + \cdots, \qquad (8.4)$$

as $R \to \infty$, where $\tilde{\theta}$ and $\tilde{\phi}$ are order-one functions of x and z. The leading-order core temperature has the constant value b determined by the boundary-layer system, this being consistent with the conditions of thermal insulation on the sidewalls and lower surface of the cavity. Substitution of (8.4) into the full governing equations (2.2) and (2.3) shows that $\tilde{\theta}$ and $\tilde{\phi}$ satisfy the equations

$$\nabla^2 \tilde{\phi} = -\frac{\partial \tilde{\theta}}{\partial x}, \quad \nabla^2 \tilde{\theta} = \frac{\partial(\tilde{\theta}, \tilde{\phi})}{\partial(x, z)}, \qquad (8.5)$$

which are, in fact, the full equations with the Darcy–Rayleigh number scaled out. On the sidewalls, the appropriate boundary conditions are

$$\tilde{\phi} = \frac{\partial \tilde{\theta}}{\partial x} = 0 \quad \text{on} \quad x = 0, L \qquad (8.6)$$

and on the lower wall

$$\tilde{\phi} = \frac{\partial \tilde{\theta}}{\partial z} = 0 \quad \text{on} \quad z = 0. \qquad (8.7)$$

Finally, the solution must match with the boundary-layer forms (5.3) and (5.1), requiring that

$$\tilde{\phi} \sim L(1-z)^{-1}p(x/L), \quad \tilde{\theta} \sim L^2(1-z)^{-3}q(x/L) \quad \text{as} \quad z \to 1 \quad \text{for} \quad 0 < x \leqslant L \quad (8.8)$$

and that

$$\tilde{\phi} \sim L(1-z)^{-1}F(\eta), \quad \tilde{\theta} \sim L^2(1-z)^{-3}G(\eta) \quad \text{as} \quad z \to 1 \quad \text{for} \quad 0 \leqslant \eta < \infty, \quad (8.9)$$

where $\eta = Lx/(1-z)^2$. The vertical boundary layer acts as a source of fluid at the upper corner ($x = 0, z = 1$) of the core, generating a weak circulation in the core (associated with order-one values of the streamfunction) which transports fluid to the lower edge of the horizontal boundary layer. The main circulation, at the order $R^{1/3}$ level of the streamfunction, is completed within the horizontal and vertical layers themselves. As far as the temperature is concerned, relative to the constant value b, there is an order R^{-1} variation in the core which, from the forms of G and $q(X)$ determined in §5, is negative near the sidewall $x = 0$ and positive elsewhere. This is consistent with the pattern of isotherms computed from the full set of equations and boundary conditions at $R = 5000$ in figure 1. The isotherm $T = b$ on which $\tilde{\theta} = 0$ emanates from the bottom of the vertical boundary layer and intersects the lower boundary of the cavity. Because of the singular nature of the core problem (8.5)–(8.9), its solution will require a careful numerical treatment and this is not attempted here. It appears, however, that this region will complete the overall asymptotic structure in the limit of large Darcy–Rayleigh number and have a solution which matches consistently with both the horizontal and vertical boundary-layer regions.

Corrections to the boundary-layer solutions arising from the core are of relative order $R^{-2/3}$ and are therefore at the same level as corrections in the horizontal layer arising from the neglected second-order z derivatives there and in the vertical layer from the influence of the temperature profile at the upper surface of the cavity. This explains why the leading terms found in the present work give a reasonably good approximation when $R = 5000$. Using the value $Z_\infty = 10$ as a rough guide to the depth of the boundary layers suggests that for this depth to be small compared with the depth of the cavity requires $10R^{-1/3}L^{2/3} \ll 1$ which, for a square cavity, is equivalent to $R \gg 1000$.

The structure identified here is expected to be relevant in other more complex cavity flows where the horizontal surfaces are thermally conducting. The present theory for flow driven from above by a buoyancy sink applies equally to flows driven from below by a buoyancy source (via the transformation $T \to 1 - T, \psi \to \psi, x \to L - x, z \to 1 - z$), of interest in relation to motions generated within geothermal energy reservoirs. The sidewall conditions $\psi = \partial T/\partial x = 0$ assumed here are the same as those applicable on the plane of symmetry of a two-dimensional plume driven by symmetrical heating from below, as discussed by Phillips (1991, §7.6). In this plume problem, the ambient temperature is generally viewed as specified at a level below that of the heat source and there is a net upward heat flux through the system, whereas, in the problem studied here, the net vertical heat flux is zero and the ambient core temperature is determined as part of the solution. Near the sidewall, where the vertical thermal gradient is negative, the flow studied here is equivalent to that of a plume, but for general plume flows with net upward heat flux, the large Z structure is expected to be different from that of §5. It is hoped to consider the structure of such flows in future work.

REFERENCES

ANSARI, A. & DANIELS, P. G. 1993 Thermally driven tall cavity flows in porous media. *Proc. R. Soc. Lond.* A **433**, 163–181.

ANSARI, A. & DANIELS, P. G. 1994 Thermally driven tall cavity flows in porous media: the convective regime. *Proc. R. Soc. Lond.* A **444**, 375–388.

BLYTHE, P. A., DANIELS, P. G. & SIMPKINS, P. G. 1982 Thermally driven cavity flows in porous media I. The vertical boundary layer structure near the corners. *Proc. R. Soc. Lond.* A **380**, 119–136.

CHANG, I. D. & CHENG, P. 1983 Matched asymptotic expansions for free convection about an impermeable horizontal surface in a porous medium. *Intl J. Heat Mass Transfer* **26**, 163–173.

CHENG, P. & CHANG, I. D. 1976 On buoyancy induced flows in a saturated porous medium adjacent to impermeable horizontal surfaces. *Intl J. Heat Mass Transfer* **19**, 1267–1272.

CHENG, P. & MINKOWYCZ, W. J. 1977 Free convection about a vertical flat plate embedded in a porous medium with application to heat transfer from a dike. *J. Geophys. Res.* **82**, 2040–2044.

DANIELS, P. G. 1983 A numerical solution of the vertical boundary-layer equations in a horizontally heated porous cavity. *J. Engng Maths* **17**, 285–300.

DANIELS, P. G., BLYTHE, P. A. & SIMPKINS, P. G. 1982 Thermally driven cavity flows in porous media II. The horizontal boundary layer structure. *Proc. R. Soc. Lond.* A **382**, 135–154.

DANIELS, P. G., BLYTHE, P. A. & SIMPKINS, P. G. 1986 Thermally driven shallow cavity flows in porous media: the intermediate regime. *Proc. R. Soc. Lond.* A **406**, 263–285.

DANIELS, P. G., BLYTHE, P. A. & SIMPKINS, P. G. 1989 Thermally driven cavity flows in porous media: the merged layer regime. *Proc. R. Soc. Lond.* A **426**, 107–124.

DANIELS, P. G. & PUNPOCHA, M. 2004 Cavity flow in a porous medium driven by differential heating. *Intl J. Heat Mass Transfer* **47**, 3017–3030.

GILL, A. E. 1966 The boundary-layer regime for convection in a rectangular cavity. *J. Fluid Mech.* **26**, 515–536.

INGHAM, D. B. & BROWN, S. N. 1986 Flow past a suddenly heated vertical plate in a porous medium. *Proc. R. Soc. Lond.* A **403**, 51–80.

INGHAM, D. B., MERKIN, J. H. & POP, I. 1982 Flow past a suddenly cooled vertical flat surface in a saturated porous medium. *Intl J. Heat Mass Transfer* **25**, 1916–1919.

JOSHI, V. & GEBHART, B. 1984 Vertical natural convection flows in porous media: calculations of improved accuracy. *Intl J. Heat Mass Transfer* **27**, 69–75.

MERKIN, J. H. 1980 Mixed convection boundary layer flow on a vertical surface in a saturated porous medium. *J. Engng Maths* **14**, 301–313.

PHILLIPS, O. M. 1991 *Flow and Reactions in Permeable Rocks*. Cambridge University Press.

WALKER, K. L. & HOMSY, G. M. 1978 Convection in a porous cavity. *J. Fluid Mech.* **87**, 449–474.

WEBER, J. E. 1975 The boundary-layer regime for convection in a vertical porous layer. *Intl J. Heat Mass Transfer* **18**, 569–573.